Journal of Hazardous Materials 162 (2009) 577–587

Contents lists available at ScienceDirect

Journal of Hazardous Materials

journal homepage: www.elsevier.com/locate/jhazmat

Review

Investigation of process performance and fouling mechanisms in micellar-enhanced ultrafiltration of nickel-contaminated waters

Ummuhan Danis[a,*], Coskun Aydiner[b]

[a] Faculty of Engineering, Department of Environmental Engineering, Atatürk University, 25240 Erzurum, Turkey
[b] Department of Environmental Engineering, Gebze Institute of Technology, Gebze 41400, Kocaeli, Turkey

ARTICLE INFO

Article history:
Received 7 February 2008
Received in revised form 21 April 2008
Accepted 21 May 2008
Available online 27 May 2008

Keywords:
Micellar-enhanced
Ultrafiltration
Nickel
Treatment
Modeling
Fouling

ABSTRACT

Nickel removal from aqueous solution by micellar-enhanced ultrafiltration (MEUF) with relatively low transmembrane pressures was investigated at varying conditions of sodium lauryl ether sulfate (SLES) and nickel concentrations, transmembrane pressure and sodium chloride content. Process employed in continuous filtration mode, could be operated within a short time of 30 min presenting high rejection of nickel and SLES at high transient fluxes. Under the effect of increasing transmembrane pressure, the rejection of nickel and SLES increased, but the transient flux decreased. The existence of salt caused to decrease both rejections and flux. Nickel rejection, SLES rejection and flux were establihed as 98.6%, 75.7% and 0.304 m^3/m^2 h, respectively, for the conditions of surfactant to metal (S/M) ratio of 10 (SLES = 2 mM), transmembrane pressure of 250 kPa without NaCl content at the end of 90-min operation time. The analyses related to the membrane fouling were carried out using adsorptive fouling models. It has been determined that, the fouling occurs as a dynamic function of various process conditions studied, and depends strongly on mechanisms controlled by the formation of gel layer and its bridging over the pore entrances simultaneously together with partial constriction of membrane pores by surfactant adsorption.

Contents

1. Introduction

Surfactants which reduce surface tension in water and other liquids, compose roughly spherical aggregates in micellar forms which contain about 50–150 molecules. The interior of micelles contain hydrocarbon chains causing a hydrophobic environment [1–3]. This feature of the surfactants brings about their preferability for industrial usages in a wide variety. The surfactants are used for various purposes in metal processing, textile, food, pharmaceuticals and paper industries [4]. They can be also used as an additive material for preconcentration and separation of metal ions and other toxic substances from water and wastewater [5]. One of the most

* Corresponding author. Tel.: +90 442 2314820; fax: +90 442 2360957.
E-mail address: ummuhanster@gmail.com (U. Danis).

0304-3894/$ – see front matter © 2008 Elsevier B.V. All rights reserved.
doi:10.1016/j.jhazmat.2008.05.098

Nomenclature

a	flux model constant (s^2/m^2)
A_m	membrane filtration area (m^2)
b	flux model constant (s/m^2)
CMC	critical micelle concentration (mM)
C_{Nf}	nickel concentration in the feed (mM)
C_{Np}	nickel concentration in the permeate (mM)
C_{Sf}	surfactant concentration in the feed (mM)
C_{Sp}	surfactant concentration in the permeate (mM)
J	permeate flux (m^3/m^2 h)
J_0	initial permeate flux (m^3/m^2 h)
k	mass transfer coefficient (s^{1-n}/m^{n-2})
K_a	mass transfer coefficient for adsorptive fouling (h^{-1})
K_b	mass transfer coefficient for complete pore blocking (h^{-1})
K_c	mass transfer coefficient for cake filtration (h/m^2)
K_i	mass transfer coefficient for intermediate blocking (m^{-1})
K_iJ_0/K_a	the normalized mass transfer coefficient for intermediate-adsorption model
$K_cJ_0^2/K_a$	the normalized mass transfer coefficient for cake-adsorption model
M	metal concentration in the feed (mM)
n	filtration constant for Hermia's equation
ΔP	transmembrane pressure (kPa)
r^2	correlation
RMSE	root mean squared error (m^3/m^2 h)
R_M	membrane hydrodynamic resistance (m^{-1})
R_N	nickel rejection (%)
R_S	surfactant rejection (%)
R_T	total resistance in membrane (m^{-1})
S	surfactant concentration in the feed (mM)
t	filtration time (h)
V	the permeate volume per unit filtration area (m^3/m^2)
V_p	total permeate volume (m^3)

Greek letters

α	specific cake resistance (m/kg)
μ	dynamic viscosity of the solution (mPa s)

common surfactant application is the micellar-enhanced ultrafiltration (MEUF) which involves the addition of the surfactant to a polluted water stream in order to promote the removal of target pollutant. MEUF is employed for improving the selectivity of inorganic ions as well as liquid membranes and polymer-enhanced ultrafiltration (PEUF) [6]. Process can be assorted into two distinct groups depending on the separation through binding of solute ions onto surface of the micelles or the disengagement of solute ions from other molecules by means of solubilisation into the micelles [7]. The polluted solution is treated by ultrafiltration membrane with pore size small enough to block the passage of micelles, depending on physico-chemical interactions among solute ions and surfactant aggregates [8,9]. The main advantages in MEUF are simple operation, high removal efficiency, low-energy requirement and pollutant recovery [9,10]. Besides, a great deal of cost effectiveness can be acquired in subsequent treatment compared with the direct treatment of the feed solution [11]. MEUF has been succesfully employed in removal of ions such as Cr^{6+} [2], Cr^{3+} [10,12], Zn^{2+} [7,10,13–15], Al^{3+} [7], Cd^{2+} [9,14,15], Cs^{+} [10], Sr^{2+} [10], Mn^{2+} [10], Co^{2+} [10], Cu^{2+} [10,13–16], Ni^{2+} [11,14,17], Au^{3+} [18], As^{5+} [19], Pb^{2+} [14], CrO_4^{2-} [8,20–22], $Fe(CN)_6^{3-}$ [8] and platinum group metals (PGMs) [23]. Process is applied over the critical micelle concentration (CMC) so as to form large metal-surfactant structures by binding metal ions. The key parameter for the success of the process is the sorption characteristics [7,14].

MEUF and PEUF are mainly known as colloid-enhanced ultrafiltration (CEUF), and PEUF consists of polymer-assisted metal complexation process occurring simultaneously with ultrafiltration. In the process, polymer material is used instead of surfactant, and the process has same advantages of MEUF. Besides, the joint use of various surfactants or polymers in each process can provide selective removal of metal ions from water environment [24,25]. Although both processes can be operated with high metal rejection rates, their major drawbacks are leakage of surfactant monomer or polyelectrolyte with lower molecular weight than molecular weight cut-off of the membrane [25,26]. CEUF processes are not already widely utilized on industrial scale, and pursue their developments due to continuing scientific researches.

Nowadays, the economic operation of the membrane processes draws attention to achieve lower costs, in practice. Therein, the employment in lower transmembrane pressures of the selected membrane application is to be important with regard to high flux achievement, as well as obtaining the permeate in very high quality. This present tendency emergent from technological viewpoint brings about the explanation of dynamic relations among process performance and membrane fouling for more effective operation of membrane separation processes in real-sized applications. This subject has been emphasized in a recent committee report of American Water Works Association (AWWA) which pointed out that the researches need to continue in order to better understand the relationships between feed water quality, pretreatment chemicals and membrane performance with the membrane fouling [27].

Nickel is of the most important ones of heavy metals in terms of environmental pollution. It is the one of the priority heavy metal pollutants which causes to serious health hazards such as contamination of water supplies, accumulation in the food chain and persistence in the nature [28,29]. Hence, in this work, it was aimed to remove nickel from waters respect to other divalent cations. Nickel is widely used in silver refineries, electroplating, zinc base casting and storage battery industries. Its concentrations in industrial wastewaters range from 3.4 to 900 mg/L and its maximum contaminant limit in potable water in accordance with the standards of European Community is 50 μg/L [5,30,31]. MEUF process can be operated with a higher performance than 90% for heavy metal removal. Therefore it can be possibly utilized in the advanced treatment of nickel-contaminated waters.

This work has been focused on the removal of nickel ions from aqueous solution using MEUF operated relatively at low transmembrane pressure. MEUF of nickel-contaminated waters was explored with aim to explain the membrane fouling together with the variations in the process performance for various operation conditions. The process was operated in a continuous cross-flow mode and the experiments were conducted at varying conditions of sodium lauryl ether sulfate (SLES) and nickel concentrations, transmembrane pressure and electrolyte content. Surfactant and metal rejections and transient flux were considered as performance parameters of the process. The modified fouling index (MFI) and specific cake resistance (α) were taken into account as characteristic parameters for the membrane fouling. Analyses of fouling behaviors according to various process conditions were comprehensively carried out by adsorptive fouling model combined with various pore blocking models.

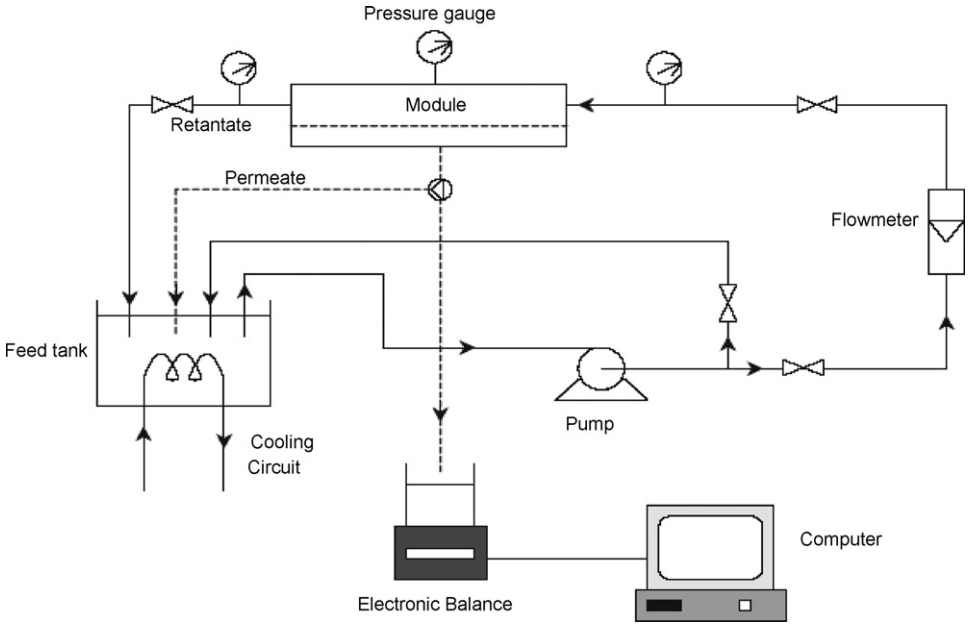

Fig. 1. Experimental set-up of continuous cross-flow microfiltration unit.

2. Materials and methods

2.1. Materials

Ultrafilters used (supplied by Schleicher & Schuell) were polycarbonate membranes with a pore diameter of 0.1 μm. SLES ($C_{12}H_{25}$–O–$(CH_2CH_2O)_2$–SO_3Na) with 384 g/mol average molecular weight and analytical-grades ($NiSO_4{\cdot}6H_2O$ and NaCl) were obtained from Merck. Anionic surfactant was used as received without further purification. CMC value of SLES had been reported as approximately 0.78 mM without changing significantly in the range of 10–40 °C [3,32].

The experiments were executed in four stages comprising the variations of surfactant concentration, nickel concentration, transmembrane pressure and electrolyte content, respectively. In the first stage, SLES concentration was chosen 0.12, 0.17, 0.2, 2, 20, 40 and 100 mM while nickel concentration was held constant at 0.2 mM. In the second stage, the process was operated at nickel concentrations of 3.2, 0.8, 0.2 and 0.05 mM for a constant surfactant concentration of 2 mM. In subsequent stages, transmembrane pressure and electrolyte content were studied at values of 150, 200 and 250 kPa and of 0, 5.7 and 22 mM for constant values of surfactant and nickel concentrations as 2 and 0.2 mM, respectively.

Table 1
Viscosity of the feed solutions for different surfactant concentrations

Surfactant solution (mM SLES)	Viscosity (mPa s)
Without surfactant (pure water)	1.000
0.12	1.004
0.17	1.006
0.2	1.030
2	1.045
20	1.080
40	1.143
100	1.443

2.2. Methods

2.2.1. Experimental procedure

Filtration equipment, shown in Fig. 1, had a feed volume of 20 L of solution. During the experiments, the feed solution which contained the known amounts of surfactant and nickel ions was pumped continuously through a cross-flow filtration cell. Process was operated at cross-flow velocity of 6 m/s and pH of 7 for all experimental runs. The temperature of feed suspension was kept constant at 30 °C by using a plate heat exchanger placed in the feed tank. The desired transmembrane pressure in filtration cell constructed from stainless steel was maintained by two manually operated valves. Flat sheat membranes of 28 cm^2 effective surface area were placed on the flat cell surface to form a one sided rectangular filtration channel of length 70 mm, width 40 mm and thickness 2 mm.

Prior to the continuous membrane filtration, the distilled water was filled into the feed tank. The feed solution was circulated to the feed tank along 30 min using by-pass line, while the filter line was shut down. Meanwhile, the desired amount of surfactant was slowly added into the feed. At the end of 30 min surfactant-recirculation period, the known amount of nikel was also added

Table 2
The adsorptive fouling models for constant pressure

Adsorptive fouling models	Mechanisms	Main equations	Fitted parameters
Adsorption	Partial pore constriction by adsorptive fouling	$J=J_0(1-K_at)^4$	K_a (h^{-1})
Cake-adsorption	Gel layer formation and adsorption	$J=J_0[(1-K_at)^{-4}+(K_cJ_0V)]^{-1}$	K_c ($h\,m^{-2}$), K_a (h^{-1})
Intermediate-adsorption	Pore blocking by bridging and adsorption	$J=J_0[(\exp(-K_iV))(1-K_at)^4]$	K_i (m^{-1}), K_a (h^{-1})
Complete-adsorption	Pore blocking by clogging and adsorption	$J=J_0\left[\left(1-\frac{K_bV}{J_0}\right)(1-K_at)^4\right]$	K_b (h^{-1}), K_a (h^{-1})

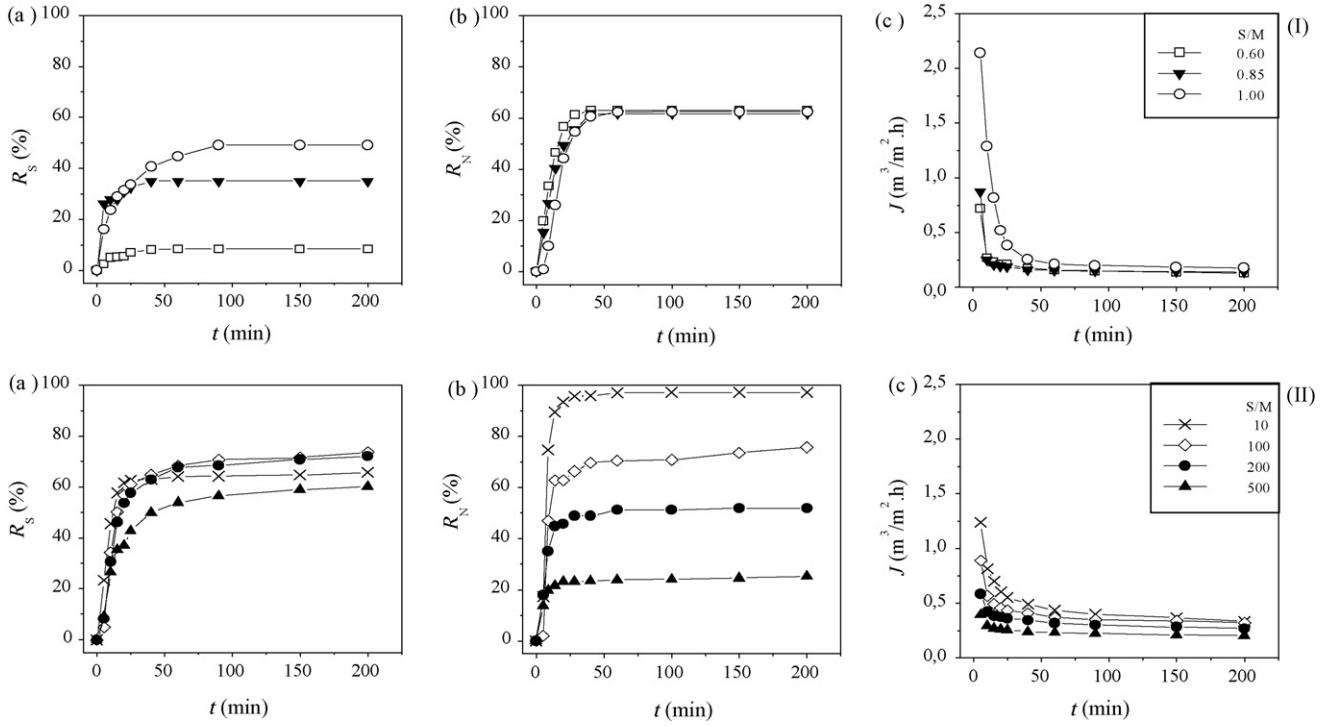

Fig. 2. The variations of rejections and transient flux with time as a function of surfactant/metal ratio at Ni = 0.2 mM. (a) SLES rejection, (b) nickel rejection and (c) transient flux ((I), under the CMC; (II), above the CMC)).

into the feed. The recirculation of surfactant and metal was applied in order to be able to obtain desirable metal rejection throughout subsequent filtration mode as a pre-process leading to the attachment of metal ions by surfactant micelles. The recirculation was continued for the following 10 min, before starting to the filtration process. At the end of 40 min full-recirculation period, the process was passed to the continuous filtration mode by opening the filter line. The desired cross-flow velocity and transmembrane pressure were obtained by preadjustment of the valves. The permeate was returned to the feed tank to obtain constant feed conditions. During filtration, feed flow rate, pH and temperature were monitored and kept constant. Permeate flow rate was measured with a balance (OHAUS-Explorer EP2101 model) at different time intervals and recorded on the computer throughout the filtration. Permeate flux was determined using a numerical differentiation method by considering the weight change of permeate on the balance. The permeate samples were also collected at different time intervals for the analyses of nickel and surfactant concentrations. For the next experiment, the valves positions were adjusted to obtain the desired cross-flow velocity and the transmembrane pressure. A new membrane with pore size of 0.1 μm made from polycarbonate was used in each experiment.

2.2.2. Analyses

The concentrations of Ni ions in the feed and the permeate were detected by Shimadzu UV 160 A model spectrophotometer at wavelength of 408 nm according to the method proposed by Lear and Mellon [33]. Reproducibility was confirmed as ±0.5%. The analysis of SLES concentrations was carried out by means of titration of aqueous samples using 0.004 N Hyamine 1622 according to American Society for Testing and Materials (ASTM) method D3049–89 [34]. The results in these samples were also checked by measurement of total organic carbon using Organic Carbon Analyser (Beckman 915 A) with UNICAM 4815 computing integrator. Reproducibility was confirmed as ±0.8%. Viscosity of the feed solutions presented in Table 1 for different feed surfactant concentrations was measured by Brookfield LVDV-E Viscometer. Viscosity values of the solutions with electrolyte content at surfactant concentration of 2 mM were virtually found same as that of without NaCl (Table 1). Viscosity of the solutions was used for the calculation of specific cake resistance (α) in Eq. (4).

2.2.3. Theoretical background

2.2.3.1. Surfactant and metal rejections. The efficiency of filtration processes is defined by conventional rejection coefficients. In this sense, the effectiveness of MEUF process was evaluated in terms of SLES and nikel rejections which were determined using the following equations, respectively:

$$R_S = 1 - \left(\frac{C_{Sp}}{C_{Sf}}\right) \quad (1)$$

$$R_N = 1 - \left(\frac{C_{Np}}{C_{Nf}}\right) \quad (2)$$

where R_S and R_N, are the rejections, C_{Sp} and C_{Np}, the concentrations in permeate and C_{Sf} and C_{Nf}, are the concentrations in feed solution for SLES and nikel, respectively.

The process performance and the membrane fouling were assessed by using S/M ratio, where S and M are identified as the initial SLES and nickel concentrations in the feed, respectively.

2.2.3.2. Flux modeling. The permeate flux in the ultrafiltration is calculated using Darcy equation [35].

$$J = \left(\frac{1}{A_m}\right)\left(\frac{dV_p}{dt}\right) = \left(\frac{\Delta P}{\mu R_T}\right) \quad (3)$$

where J, permeate flux; A_m, membrane filtration area; V_p, total permeate volume; t, filtration time; ΔP, transmembrane pressure; μ, dynamic viscosity of the solution; R_T, total membrane resistance.

At the scope of the study, flux data obtained from the experiments were modeled using the following equation [36]:

$$J = \left[\left(\frac{\mu R_M}{\Delta P}\right)^2 + \left(\frac{2C_{Sf}\alpha\mu}{\Delta P}\right)t\right]^{-1/2} \quad (4)$$

where R_M is the membrane hydrodynamic resistance. Eq. (4) can also be expressed in the form of $J=(a+bt)^{-1/2}$. Model constants (a and b) are determined by means of non-linear curve fitting of experimental J data obtained versus time using Eq. (4). The regression calculations were made using SigmaPlot 9.01 (Systat Software Inc.), and the agreements between the modeled and the regressed values of J versus time were evaluated in terms of r^2 and root mean squared error (RMSE).

2.2.3.3. Membrane fouling analyses. In membrane processes, the membrane fouling was basically identified by means of modified fouling index parameter which is determined from the gradient of linear region of the plot of t/V versus V, using general cake filtration equation in constant pressure [35].

$$\frac{t}{V} = \left(\frac{\mu R_M}{\Delta P}\right) + \left(\frac{\mu\alpha C_{Sf}V}{2\Delta P}\right) \quad (5)$$

where V is the permeate volume per unit filtration area. In the study, MFI was calculated as one forth of b constant in Eq. (4), to be an indicator for the whole process, not only for linear region in t/V plot in Eq. (5). In addition, α, representing the hydrodynamic resistance to the flow due to the membrane fouling, was taken into account as the parameter describing the main characteristics of the gel layer and was determined from b constant in Eq. (4). α is defined as the resistance per unit thickness of gel layer and, is stated as the reciprocal relationship with average diameter of aggregates and porosity in layer according to Carmen–Kozeny equation [37].

Analyses depending on the fouling mechanisms were carried out using membrane blocking models, which were combined with adsorptive fouling model assuming that foulant deposition on the membrane has zeroth-order kinetics. Membrane blocking models are identified by the blocking laws which describe the transition mechanisms from pore blocking to cake formation. These mechanisms are generally expressed with a physical model developed by Hermia as follows [38]:

$$\frac{d^2t}{dV^2} = k\left(\frac{dt}{dV}\right)^n \quad (6)$$

where k and n are the mass transfer coefficient and the filtration constant, respectively. The values of n as 0, 1, 1.5 and 2 define cake, intermediate, standard and complete blocking filtration, respectively. Eq. (6) is frequently used to explain the filtration mechanisms using experimental data obtained from the membrane filtration. Besides, Bolton et al. [39] developed a new adsorption model which was be able to incorporate into the blocking models. While standard pore blocking model assumes transition of all the foulant into the membrane pores, this model assumes the deposition of some fractions of foulant and was succesfully applied to the purification of protein therapeutics [39]. Within this framework, the fouling dynamics in MEUF of nickel solutions were elaborately investigated by single adsorption model and combined adsorption models as cake-adsorption, intermediate-adsorption and complete-adsorption. The main equations and descriptive mechanisms related to the models used were presented in Table 2.

Table 3
The results obtained for the membrane fouling at various S/M ratios for Ni = 0.2 mM and t = 200 min

C_{Sf}/C_{Nf}	Flux model						Fouling models										
							Cake-adsorption				Intermediate-adsorption				Normalized mass transfer coefficients		
	a (s^2/m^2)	b (s/m^2)	r^2	RMSE	MFI (s/m^2)	α ($\times10^{12}$ m/kg)	K_c	K_a	r^2	RMSE	K_i	K_a	r^2	RMSE	KC_0^2/K_a	KJ_0/K_a	
0.60	208,641	210,789	0.993	0.0114	52,697	329.08	23.63	1.47	0.998	0.099	23.80	2.36	0.996	0.148	1000.4	79.6	
0.85	208,641	210,789	0.967	0.0140	52,697	232.24	17.68	1.57	0.997	0.132	20.12	1.91	0.997	0.124	699.6	83.1	
1	25,828	25,779	0.852	0.0529	6,445	24.14	2.69	0.94	0.999	0.217	12.03	4.04×10^{-8}	0.997	0.359	1441.2	6.67×10^{9}	
10	25,048	26,583	0.992	0.0266	6,646	2.42	6.34	0.87	0.999	0.237	12.97	3.92	0.996	0.468	3691.0	74.5	
100	51,851	51,355	0.990	0.0327	12,839	0.44	12.09	0.90	0.998	0.224	16.90	4.00	0.995	0.356	3361.0	66.9	
200	77,111	77,419	0.979	0.0301	19,355	0.30	24.78	1.41×10^{-6}	0.998	0.185	24.44	4.78	0.995	0.279	2.95×10^{9}	66.3	
500	152,906	155,628	0.992	0.0232	38,907	0.20	52.72	1.77×10^{-6}	0.998	0.141	35.82	4.92	0.995	0.201	2.52×10^{9}	67.1	

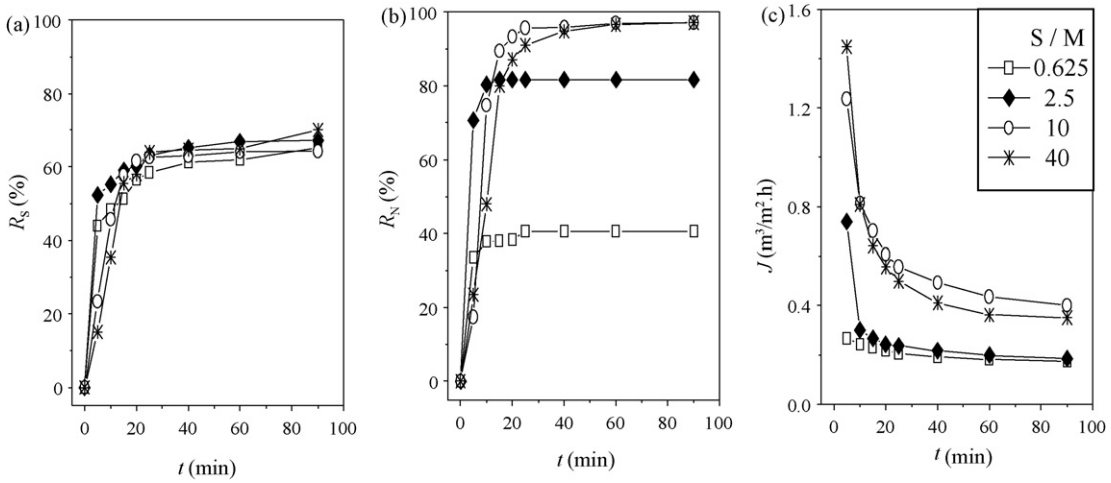

Fig. 3. The variations of rejections and transient flux with time as a function of surfactant/metal ratio at SLES = 2 mM. (a) SLES rejection, (b) nickel rejection and (c) transient flux.

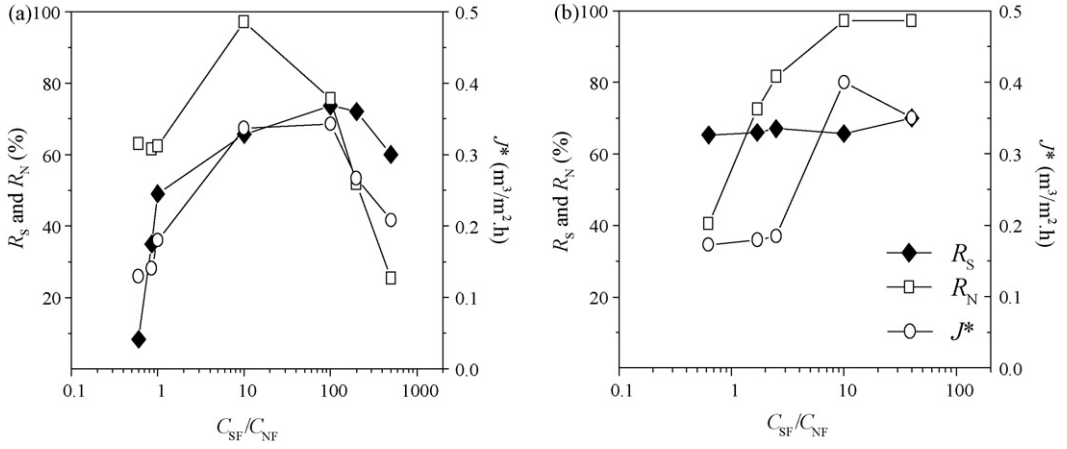

Fig. 4. The variations of rejections and transient flux with varying *S*/*M* ratio, (a) Ni = 0.2 mM and *t* = 200 min, (b) SLES = 2 mM and *t* = 90 min.

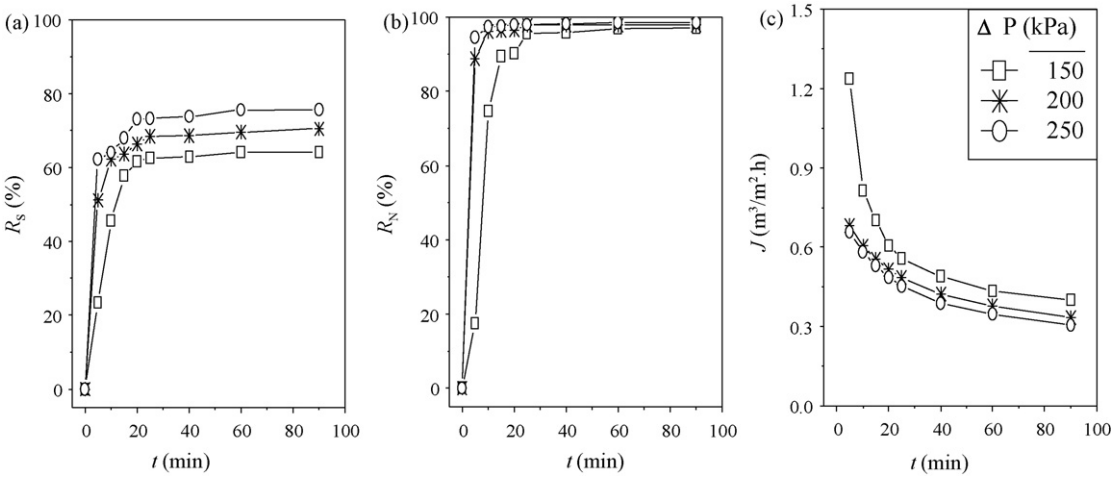

Fig. 5. The variations of rejections and transient flux with time as a function of transmembrane pressure at *S*/*M* = 10 mM (SLES = 2 mM). (a) SLES rejection, (b) nickel rejection and (c) transient flux.

3. Result and discussion

3.1. The influence of the variation of SLES amount

These experiments were conducted for different S/M ratios by changing SLES concentration in the feed at constant nickel concentration of 0.2 mM. The variations in SLES and nickel rejections and permeate flux versus time are presented in Fig. 2.

Both rejections first increased then decreased by increasing of S/M ratio from 0.6 to 500. S/M ratios of 10 and 100 were obtained for the nickel rejection and the flux and, the SLES rejection, respectively, as turning points where process apparently exhibited best performance. Besides, relative steady-state times were approximately established as 75, 25 and 150 min for SLES, nickel and flux, respectively. In spite of crucial rejection increments in a few minutes of the experiments, noticeable decrements in the flux were observed. On the other hand, while considerable flux decrements were not seen for the range of 1–100 S/M ratio, the both rejections performed remarkable alterations. In $S/M = 10$ case, both nickel rejection and the flux reached the highest levels of 97.2% and 0.335 m^3/m^2 h at the end of the filtration time, respectively. Whereas, SLES rejection was obtained as 65.7%. It was understood that, the amount of nickel-bound micelles reached a maximum at $S/M = 10$, and this caused to the lowest amount of free nickel ions in the feed. However, this situation brings about more complicated evaluations. It has been reported in the literature that, the increment in surfactant concentration results in an increase in the micelle size and, the shapes of the micelles transform from spherical to lamellar even the active charge of micelles decreases [22]. It can be accordingly said that, spherical micelles transformed lamellar forms at high SLES concentrations, especially after S/M of 10. This formal transformation in micelle structures gave rise to decrease of nickel amount bound with SLES micelles, because of decreasing of active charges of micelles and thus of passing of nickel ions to the permeate together with lower molecular-weigthed surfactant micelles. Consequently, this breakthrough in surfactant concentration confers a marked advantage for reduction of surfactant consumption in the application of the process.

Comprehensive analyses concerning the membrane fouling were carried out by evaluating of the results obtained from adsorptive fouling models, given in Table 3.

In the membrane fouling analyses, both single adsorption and complete-adsorption models did not present any or meaningful correlations with experimental data. Accordingly, it can be said that, the fouling in the membrane occurred as a stand-alone function of neither partial pore constriction nor blocking of pore entrances by surfactant aggregates. Besides, cake-adsorption and intermediate-adsorption combined models presented admirably good correlations in terms of r^2 and RMSE values. The results depicted in Table 3 mean that, the membrane fouling can be designated by the gel layer formation and the blocking over pores by bridging of aggregates for cake-adsorption and intermediate-adsorption, respectively, as a simultaneous function of partial pore constriction based on adsorption of surfactant monomers and aggregates on the pore walls. α decreased as SLES concentration increased. However, the variation of MFI showed that the fouling occurred with rather different mechanisms. More porous gel layer comprising bigger aggregates formed on membrane surface because of decreasing of α values with increasing of surfactant concentration. The lower foulings were obtained for $S/M = 1$ and 10. In case of $S/M > 100$, α almost did not vary although the membrane fouling increased. All of these results supported that micelle sizes changed after $S/M = 10$. For the studied S/M ratios under (0.6, 0.85 and 1.0) and above (10, 100, 200 and 500) the CMC, the predominant mechanisms in the flux decline have been the formation of the gel layer and its bridging over the pores much more than constriction of the pores by adsorptive fouling, according to the normalized mass transfer coefficients. Besides, the formation of the gel became much more influential than its bridging the pore entrances, except for $S/M = 1$ which was observed at the lowest fouling. The main reason of the membrane fouling at $S/M = 1$ has been the increase in the bridging effect of the gel, when compared with its existence on the membrane surface. However, the increase of the fouling as proportional with this effect was probably hindered due to increasing of gel porosity and aggregate diameters in the secondary layer. On the other hand, while the existence of the gel layer on the membrane surface caused to more foulings in case of $S/M \geq 10$, there have almost been no variation in its bridging influence.

3.2. The influence of the variation of nickel amount

In these experiments, different S/M ratios in the feed were studied by changing the nickel concentration at constant SLES concentration of 2 mM. The variations of SLES and nickel rejections and permeate flux versus time are depicted in Fig. 3.

Fig. 3 indicates that the increase of nickel concentration does not significantly affect SLES rejection (64.2–70%), while remarkable increases in nickel rejection can be obtained. Process reaches to rel-

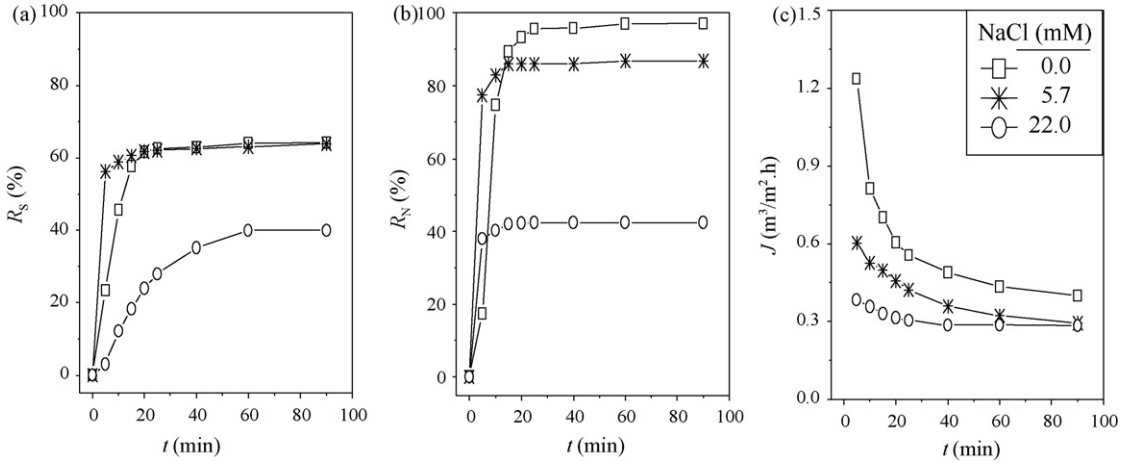

Fig. 6. The variations of rejections and transient flux with time as a function of NaCl concentration at $S/M = 10$ mM (SLES = 2 mM). (a) SLES rejection, (b) nickel rejection and (c) transient flux.

ative steady-states at times of 40 and 90 min for both rejections and the flux, respectively. $S/M = 10$ has been the turning point that leads to changing process performance in purification of nickel ions by MEUF. At $S/M = 10$, nickel rejection and the flux were determined as 97.2% and 0.4 m^3/m^2 h, respectively. Higher transient fluxes were appeared at $S/M = 10$ and 40, compared to other two conditions studied. The variations of rejections and transient flux versus various S/M ratios for SLES and nickel concentrations of 2 and 0.2 mM are also presented in Fig. 4(a) and (b), respectively.

Noticeable differences in nickel rejection and flux are observed for under and above $S/M = 10$. In MEUF of nickel-contaminated waters, the use of surfactant above the CMC provided to obtain higher rejections and fluxes than those under the CMC at the end of the studied process times. The results obtained from modeling of experimental fluxes in Fig. 3(c) were used in order to elaborately interpret the reasons of the membrane fouling causing to flux decline and are shown in Table 4.

Meaningful correlations did not obtain for single adsorption model, while complete-adsorption model represented partially acceptable predictions. Predominant mechanisms were determined to be intermediate-adsorption, cake-adsorption and complete-adsorption, respectively, from the normalized mass transfer coefficients determined for 90-min filtration time. The bridging of the gel layer over the pore openings became much more influential way on the membrane fouling than, respectively, the gel formation and the blocking of pore entrances by aggregates of equivalent to pore size. Partial pore constriction by adsorption performed the lowest effect when compared with its combined effects. The lower foulings, which lead to the lower α values representing a gel layer with more porous and bigger aggregate diameter, were observed at $S/M = 10$ and 40. This put forward that, as nickel amount in the feed decreased, the membrane fouling has been mainly a function of the gel properties, not the gel occurrence and its bridging over the pores.

3.3. The influence of the variation of transmembrane pressure

The operation of membrane process at low transmembrane pressures is an important issue in terms of decreasing the operating costs. Thus, a set of three experiments representing relatively low transmembrane pressures ($\Delta P = 150$, 200 and 250 kPa) was conducted at $S/M = 10$ (SLES = 2 mM). The results considering SLES and nickel rejections and permeate flux versus time are presented in Fig. 5.

From the figure it can be seen as transmembrane pressure increases, both rejections increases, but transient flux decreases. The increment in SLES rejection occurres as more distinctive than that of nickel. Higher permeate fluxes are achieved at lower transmembrane pressure even at the very beginning of the experiment. In case of 250 kPa, nickel rejection, SLES rejection and the flux are established as 98.6%, 75.7% and 0.304 m^3/m^2 h, respectively. Unfortunately, very high surfactant rejection could not be obtained for the conditions studied thus far. It is well known that surfactant rejection is rather crucial to economically operate MEUF process in real-sized applications. At this frame, it can be suggested to use the membrane with lower pore size or the binary surfactant for the purpose of obtaining higher surfactant rejection at relatively low transmembrane pressures. However, it can be taken into account that, the use of ultrafilter membranes with relatively lower molecular weight cut-off would ensure flexibility in application due to difficulties to be originated from using of binary surfactant in terms of recovery and reuse.

The results related to the membrane fouling and the adsorptive fouling models under the influence of transmembrane pressure are depicted in Table 5.

Table 4
The results obtained for the membrane fouling at various S/M ratios for SLES = 2 mM and $t = 90$ min

C_{Sf}/C_{Nf}	Flux model					Fouling models															
	a (s^2/m^2)	b (s/m^2)	r^2	RMSE	MFI (s/m^2)	α ($\times 10^{12}$ m/kg)	Cake-adsorption				Intermediate-adsorption				Complete-adsorption				Normalized mass transfer coefficients		
							K_c	K_a	r^2	RMSE	K_i	K_a	r^2	RMSE	K_b	K_a	r^2	RMSE	Kc_0^2/K_a	K_iJ_0/K_a	K_b/K_a
0.625	202,221	210,789	0.995	0.0153	52,697	18.02	105.33	0.93	0.998	0.129	149.13	6.37×10^{-6}	0.995	0.205	157.83	0.99	0.763	1.351	7235.6	1.87×10^8	159.6
2.5	204,302	208,641	0.995	0.0155	52,160	17.84	23.78	0.94	0.998	0.124	37.04	2.79×10^{-8}	0.996	0.174	81.39	0.92	0.917	0.787	1606.9	1.06×10^{10}	88.6
10	24,367	27,288	0.992	0.0196	6,822	2.33	6.46	0.90	0.999	0.238	26.77	3.29×10^{-7}	0.995	0.542	119.02	0.93	0.841	3.186	3814.5	1.88×10^9	127.7
40	37,501	36,544	0.979	0.0149	9,136	3.12	5.31	0.93	0.999	0.179	19.57	1.00×10^{-7}	0.995	0.434	88.26	0.943	0.888	2.148	1973.8	3.64×10^9	94.4

Table 5
The results related to the membrane fouling at various transmembrane pressures for $S/M = 10$ (SLES = 2 mM) and $t = 90$ min

ΔP (kPa)	Flux model						Fouling models													
	a (s^2/m^2)	b (s/m^2)	r^2	RMSE	MFI (s/m^2)	α ($\times 10^{12}$ m/kg)	Cake-adsorption				Intermediate-adsorption				Complete-adsorption				Normalized mass transfer coefficients		
							K_c	K_a	r^2	RMSE	K_i	K_a	r^2	RMSE	K_b	K_a	r^2	RMSE	$K_c J_0^2/K_a$	$K_i J_0/K_a$	K_b/K_a
150	24,367	27,288	0.992	0.0196	6,822	2.33	6.46	0.90	0.999	0.238	26.77	3.29×10^{-7}	0.995	0.542	119.02	0.93	0.841	3.186	3814.5	1.88×10^{9}	127.7
200	51,856	51,355	0.982	0.0272	12,839	4.39	16.33	2.40×10^{-6}	0.998	0.242	53.33	3.41×10^{-6}	0.993	0.470	120.08	0.93	0.754	2.710	1.70×10^{9}	2.47×10^{8}	129.1
250	51,856	51,355	0.987	0.0200	12,839	4.39	18.17	0.86	0.998	0.255	56.08	3.43×10^{-6}	0.994	0.442	126.12	0.93	0.759	2.686	5280.3	2.58×10^{8}	135.6

Table 6
The results related to the membrane fouling at various NaCl concentrations for $S/M = 10$ (SLES = 2 mM) and $t = 90$ min

NaCl (mM)	Flux model						Fouling models													
	a (s^2/m^2)	b (s/m^2)	r^2	RMSE	MFI (s/m^2)	α ($\times 10^{12}$ m/kg)	Cake-adsorption				Intermediate-adsorption				Complete-adsorption				Normalized mass transfer coefficients		
							K_c	K_a	r^2	RMSE	K_i	K_a	r^2	RMSE	K_b	K_a	r^2	RMSE	$K_c J_0^2/K_a$	$K_i J_0/K_a$	K_b/K_a
0	24,367	27,288	0.992	0.0196	6,822	2.33	6.46	0.90	0.999	0.238	26.77	3.29×10^{-7}	0.995	0.542	119.02	0.93	0.841	3.186	3814.5	1.88×10^{9}	127.7
5.7	49,775	53,503	0.973	0.0198	13,376	4.57	21.68	0.86	0.998	0.241	63.59	3.37×10^{-6}	0.995	0.413	140.97	0.93	0.755	2.770	6583.5	3.05×10^{8}	151.5
22	100,590	105,931	0.947	0.0259	26,483	9.06	49.07	6.88×10^{-6}	0.998	0.189	103.17	8.37×10^{-6}	0.994	0.307	148.56	0.91	0.729	2.046	9.19×10^{8}	1.40×10^{8}	162.6

According to Table 5, the lowest fouling is obtained at pressure of 150 kPa because of more porous gel layer with relatively bigger aggregates on membrane surface. The fouling increased with increasing of ΔP and, identical values are obtained for the membrane fouling and the gel properties at pressures of 200 and 250 kPa. Predominant mechanism was determined as the bridging of the gel layer the pore openings, except for 200 kPa. In case of 200 kPa, gel layer formation became more influential than pore blocking by bridging. Although different mechanisms were predominantly prevailed for 200 and 250 kPa, it was understood that the flux decline had been by reason of the bridging of pore entrances due to same fouling and gel properties determined. Like in the conditions studied until now, partial pore constriction by adsorption of surfactant monomers and aggregates performed the lowest influence on the membrane fouling. On the other hand, pore blocking by clogging of pore entrances with equivalent-sized aggregates performed a very few influence on the flux decline.

3.4. The influence of the variation of electrolyte content

Monovalent salts have been extensively used in electroplating and metal finishing processes, and thus it is enable to meet with electrolyte content in wastewaters including heavy metal pollution [11,20]. The variations in the performance of MEUF process by the addition of monovalent salt (NaCl) were therefore examined at this stage of the study and the results are shown in Fig. 6.

As depicted in Fig. 6, both rejections and transient flux decrease with increasing of electrolyte concentration, and SLES rejection is not significantly affected from low NaCl concentration. It is also shown that, the increased electrolyte concentration does not cause a significant change in the flux at the end of the process time. Salt presence in solution decreases the CMC of SLES due to decreasing of the repulsive forces between headgroups of surfactant. In other words, much micellar structures form in solution compared to the absence of the electrolyte. Besides, free Na ions also compete with Ni ions [11,15]. These reasons, which render understandable the decrement in both rejections are, however, not sufficient to elucidate the membrane fouling and the flux decline. Therefore, comprehensive analyses were conducted by using the results presented in Table 6.

The increase in the elecrolyte content of solution increases both the membrane fouling and the specific gel resistance because of the formation of relatively smaller aggregates in a less porous layer on the membrane surface. The presence of Na ions promoted the formation of micellar structures with lower size. The fouling and the flux decline occurred simultaneously under the effect of mechanisms comprising, respectively, intermediate blocking, gel layer formation, complete blocking and adsorption in the pores. Despite partial decrease in pore blocking by bridging with increasing of electrolyte concentration, the increase of the effect of the gel layer on the membrane fouling brought about considerable decreases in both rejections and the flux. Thus, it was concluded that, the determinative factor for the process performance in case of existence of electrolyte has been the gel properties, while gel formation and its bridging the pore entrances were synergistically important for the fouling.

4. Conclusions

This study was performed for investigating dynamically the performance and the fouling behavior of MEUF process under various SLES and nickel concentrations, transmembrane pressure and electrolyte content. Process was operated in a continuous filtration mode with relatively low transmembrane pressures. The following results were obtained:

1. It was established that process could reach to steady-state in approximately 30 and 90 min for SLES and nickel rejection and flux, respectively, in spite of varying process conditions. Nickel rejection, SLES rejection and flux were determined as 98.6%, 75.7% and 0.304 m^3/m^2 h, respectively, for the conditions of surfactant to metal (S/M) ratio of 10 (SLES = 2 mM), transmembrane pressure of 250 kPa without NaCl content at the end of 90-min operation time.
2. The membrane fouling depends strongly on the mechanisms based on cake-adsorption (gel layer formation and adsorption) and intermediate-adsorption (pore blocking by bridging and adsorption) blocking models. Adsorption and complete-adsorption models displayed a fairly negligible proportion on the fouling and the flux behaviors.
3. This study put forward that, for relatively more economical or feasible removal of metal ion from wastewater, MEUF process should be employed as tending to prevent the existence of the gel layer or to provide the formation of highly porous gel layer.

References

[1] R.O. Dunn, F.J. Scamehorn, O.S. Christian, Removal of *n*-alcohols from aqueous streams using micellar enhanced ultrafiltration by cationic surfactant, J. Membr. Sci. 56 (1987) 1.
[2] G. Ghosh, P.K. Bhattacharya, Hexavalent chromium ion removal through micellar enhanced ultrafiltration, J. Chem. Eng. 119 (2006) 45–53.
[3] Y. Kaya, C. Aydiner, H. Barlas, B. Keskinler, Nanofiltration of single and mixture solutions containing anionics and nonionic surfactants below their critical micelle concentrations (CMCs), J. Membr. Sci. 282 (2006) 401.
[4] D. Myers, Surfaces, Interfaces and Colloids—Principles and Applications, 2nd ed., John Wiley & Sons, New York, 1999.
[5] C. Aydiner, M. Bayramoglu, S. Kara, B. Keskinler, O. Ince, Nickel removal from waters using surfactant-enhanced hybrid PAC/MF process. I. The İnfluence of system-component variables, Ind. Eng. Chem. Res. 45 (2006) 3926.
[6] P. Canizares, A. Perez, R. Camarillo, J.J. Linares, A semi-continuous laboratory-scale polymer enhanced ultrafiltration process for the recovery of cadmium and lead from aqueous effluents, J. Membr. Sci. 240 (2004) 197.
[7] N. Hankins, N. Hilal, O.O. Ogunbiyi, B. Azzopardi, Inverted polarity micellar enhanced ultrafiltration for the treatment of heavy metal polluted wastewater, Desalination 185 (2005) 185.
[8] K. Baek, B.K. Kim, H.J. Cho, J.W. Yang, Removal characteristics of anionic metals by micellar-enhanced ultrafiltration, J. Hazard. Mater. B99 (2003) 303.
[9] X. Ke, Z. Guang-ming, H. Jin-hui, W. Jiao-yi, F. Yao-yao, H. Guohe, L. Jianbing, X. Beidou, L. Hongliang, Removal of Cd^{2+} from synthetic wastewater using micellar-enhanced ultrafiltration with hollow fiber membrane, Colloids Surf. A: Physicochem. Eng. Aspects 294 (1–3) (2007) 140.
[10] R.S. Juang, Y.Y. Xu, C.L. Chen, Separation and removal of metal ions from dilute solutions using micellar-enhanced ultrafiltration, J. Membr. Sci. 218 (2003) 257.
[11] A.J. Chhatre, K.V. Marathe, Dynamic analysis and optimization of surfactant dosage in micellar enhanced ultrafiltration of nickel from aqueous streams, Sep. Sci. Technol. 41 (2006) 2755.
[12] M. Aoudia, N. Allal, A. Djennet, L. Toumi, Dynamic micellar enhanced ultrafiltration: use of anionic (SDS)–nonionic(NPE) system to remove Cr^{3+} at low surfactant concentration, J. Membr. Sci. 217 (2003) 181.
[13] R. Juang, J. Liang, Removal of copper and zinc from aqueous sulfate solution with polyacrylic acid by a batch complexation ultrafiltration process, J. Membr. Sci. 82 (1993) 175.
[14] Y.C. Huang, B. Batchelor, S.S. Koseoglu, Cross-flow surfactant-based ultrafiltration of heavy metals from waste streams, Sep. Sci. Technol. 29 (15) (1994) 1979.
[15] J.F. Scamehorn, S.D. Christian, D.A. El-sayed, H. Uchiyama, Removal of divalent metal cations and their mixtures from aqueous streams using micellar enhanced ultrafiltration, Sep. Sci. Technol. 297 (1994) 809.
[16] C.W. Li, C.K. Liu, W.S. Yen, Micellar-enhanced ultrafiltration (MEUF) with mixed surfactants for removing Cu(II) ions, Chemosphere 63 (2006) 353.
[17] L. Yurlova, A. Kryvoruchko, B. Kornilovich, Removal of Ni(II) ions from wastewater by micellar-enhanced ultrafiltration, Desalination 144 (2002) 255.
[18] S. Akita, L. Yang, H. Takeuchi, Micellar-enhanced ultrafiltration of gold(III) with nonionic surfactant, J. Membr. Sci. 133 (1997) 189.
[19] J. Iqbal, H.J. Kim, J.S. Yang, K. Baek, Removal of arsenic from groundwater by micellar-enhanced ultrafiltration (MEUF), Chemosphere 66 (2007) 970.
[20] B. Keskinler, U. Danis, A. Cakici, G. Akay, Chromate removal from water using surfactant enhanced crossflow filtration, Sep. Sci. Technol. 32 (11) (1997) 1899.

[21] L. Gzara, M. Dhahbi, Removal of chromate anions by micellar-enhanced ultrafiltration using cationic surfactants, Desalination 137 (2001) 241.
[22] S.D. Christian, S.N. Bhat, E.E. Tucker, J.F. Scamehorn, D.A. El-Sayed, Micellar-enhanced ultrafiltration of chromate anion from aqueous streams, AIChE J. 34 (2) (1988) 189.
[23] S. Gwicana, N. Vorster, E. Jacobs, The use of a cationic surfactant for micellar-enhanced ultrafiltration of platinum group metal anions, Desalination 199 (2006) 504.
[24] J.L. Aguirre, V. Garcia, E. Pongracz, R. Keiski, Applicability of membrane technologies for the removal of heavy metals, Desalination 200 (2006) 272.
[25] Y.K. Choi, S.B. Lee, D.J. Lee, Y. Ishigami, T. Kajiuchi, Micellar enhanced ultrafiltration using PEO–PPO–PEO block copolymers, J. Membr. Sci. 148 (1998) 185.
[26] K. Baek, J.S. Yang, T.S. Kwon, J.W. Yang, Cationic starch-enhanced ultrafiltration for Cr(VI) removal, Desalination 206 (2007) 245.
[27] AWWA, Membrane Technology Research Committee, recent advances and research needs in membrane fouling, J. Am. Water Works Assoc. 97 (8) (2005) 79.
[28] AWWA, Water Desalting and Reuse Committee, membrane desalting technologies, J. Am. Water Works Assoc. 81 (11) (1989) 30.
[29] Y.K. Bayhan, B. Keskinler, A. Cakici, M. Levent, G. Akay, Removal of divalent heavy metal mixtures from water by *Saccharomyces cerevisiae* using crossflow microfiltration, Water Res. 35 (9) (2001) 2191.
[30] H. Hasar, Adsorption of nickel(II) from aqueous solution onto activated carbon prepared from almond husk, J. Hazard. Mater. B97 (2003) 49.
[31] E. Demirbas, M. Kobya, M.S. Oncel, S. Sencan, Removal of Ni(II) from aqueous solution by adsorption onto hazelnut shell activated carbon: equilibrium studies, Bioresour. Technol. 84 (2002) 291.
[32] A.C. Archer, A.M. Mendes, R.A.R. Boaventura, Separation of anionic surfactant by nanofiltration, Environ. Sci. Technol. 33 (1999) 2758.
[33] J.B. Lear, M.G. Mellon, Absorptiometric determination of nickel with beta-mecaptopropionic acid, Anal. Chem. 25 (9) (1953) 1411.
[34] American Society for Testing and Materials (ASTM), D3049–89-Standard Test Method for Synthetic Anionic Ingredient by Cationic Titration, ASTM, Philadelphia, PA, 2003.
[35] M. Mulder, Basic Principles of Membrane Technology, Kluwer Academic Publishers, Netherlands, 1991.
[36] E. Turano, S. Curcio, M.G. De Paola, V. Calabrò, G. Iorio, An integrated centrifugation–ultrafiltration system in the treatment of olive mill wastewater, J. Membr. Sci. 209 (2002) 519.
[37] Y. Lee, M.M. Clark, Modeling of flux decline during crossflow ultrafiltration of colloidal suspensions, J. Membr. Sci. 149 (1998) 181–202.
[38] J. Hermia, Constant pressure blocking filtration laws—application to power-law non-Newtonian fluids, Trans. IChemE. 60 (1982) 183.
[39] G.R. Bolton, A.W. Boesch, M.J. Lazzara, The effects of flow rate on membrane capacity: development and application of adsorptive membrane fouling models, J. Membr. Sci. 279 (2006) 625.